Eur. Phys. J. E (2014) **37**: 124
DOI 10.1140/epje/i2014-14124-0

THE EUROPEAN PHYSICAL JOURNAL E

Regular Article

Optically driven oscillations of ellipsoidal particles. Part I: Experimental observations*

B.M. Mihiretie[a], P. Snabre, J.-C. Loudet[b], and B. Pouligny

Université de Bordeaux, CNRS, Centre de Recherche Paul Pascal, Avenue A. Schweitzer, F-33600 Pessac, France

Received 15 July 2014 and Received in final form 21 October 2014
Published online: 22 December 2014 –

Abstract. We report experimental observations of the mechanical effects of light on ellipsoidal micrometre-sized dielectric particles, in water as the continuous medium. The particles, made of polystyrene, have shapes varying between near disk-like (aspect ratio $k = 0.2$) to very elongated needle-like ($k = 8$). Rather than the very tightly focused beam geometry of optical tweezers, we use a moderately focused laser beam to manipulate particles individually by optical levitation. The geometry allows us varying the longitudinal position of the particle, and to capture images perpendicular to the beam axis. Experiments show that moderate-k particles are radially trapped with their long axis lying parallel to the beam. Conversely, elongated ($k > 3$) or flattened ($k < 0.3$) ellipsoids never come to rest, and permanently "dance" around the beam, through coupled translation-rotation motions. The oscillations are shown to occur in general, be the particle in bulk water or close to a solid boundary, and may be periodic or irregular. We provide evidence for two bifurcations between static and oscillating states, at $k \approx 0.33$ and $k \approx 3$ for oblate and prolate ellipsoids, respectively. Based on a recently developed 2-dimensional ray-optics simulation (Mihiretie *et al.*, EPL **100**, 48005 (2012)), we propose a simple model that allows understanding the physical origin of the oscillations.

1 Introduction

Radiation pressure (RP) forces from a few-milliwatts laser beam are known to produce forces in the picoNewton range, well enough to levitate and manipulate a small (micrometer sized) dielectric particle [1–3]. Since the invention of laser optical tweezers (OT) [4], based on a single very large-aperture beam, considerable *savoir faire* and theoretical knowledge have been accumulated in the art of trapping and manipulating particles with light. These works have generated a huge amount of literature; see the reviews by *e.g.* [5] or [6].

However research works have dealt essentially with the simplest kind of particles namely spheres. In this case, solutions have been proposed to handle about any kind of particle, from a few tens of nanometers up to about hundreds of micrometers. Transparent spheres whose refractive index is larger than that of the surrounding medium ($n_p > n$, *i.e.* $m = n_p/n > 1$) may be trapped around the focus of a single large-aperture Gaussian beam [4–6], or between the foci of a couple of coaxial counterpropagating Gaussian beams [1,3,7–12]. Spheres made of weakly refractive matter ($m < 1$), of reflective or absorbing materials are pushed out of classical Gaussian beams, but, within certain limits, the difficulty may be circumvented by using beams with a hollow core. Laguerre-Gauss structures or optical vortex beams [13,14] and optical bottles [15–17] are well-known solutions to this problem. An alternate solution, still with a Gaussian beam, is to scan the beam to obtain a time-averaged structure that is equivalent to a hollow beam [18].

In the case of a particle made of a homogeneous isotropic non-absorbing material, the optical force may be represented as the sum of surface stresses that are everywhere perpendicular to the surface [19]. A consequence of this property is that the optical torque acting on a sphere made of a transparent isotropic material is null. Therefore the sphere cannot be made to rotate under the sole action of optical forces. The situation is very different with a non-spherical particle, since the resulting torque is not null in general. Laser light will move the particle and make it rotate in the same time. Manipulating the particle implies handling 6 degrees of freedom, 3 position coordinates (x, y, z) and 3 Euler angles.

Because of this complication, trapping of non-spherical particles is both very different and less mastered than that of spheres [20]. Little is known about possibilities

* Supplementary material in the form of four .pdf files available from the Journal web page at
http://dx.doi.org/10.1140/epje/i2014-14124-0

[a] *Present address:* Department of Physics, University of Gothenburg, Sweden.
[b] e-mail: loudet@crpp-bordeaux.cnrs.fr

to effectively trap particles of various shapes, either experimentally or theoretically. There is currently a lot of interest from physicists and engineers about trapping and manipulating elongated particles, in great part due to the proliferating applications of nanotubes and nanorods in biophysics, microfluidics, microelectronics and photonics [21–25]. A goal pursued by engineers is to assemble micron-sized structures and mechanisms made of such particles, a challenge that necessitates optical trapping and control of the orientation of individual rods [23,26].

Experimental observations and the challenge of optically manipulating non-spherical objects in general have motivated a bunch of theoretical and numerical studies in the recent years. The case of rods has been addressed along different shape variants, such as cylinders [27–30], prolate ellipsoids [31–33] or chains of spheres [34]. Cao *et al.* recently carried out a systematic study of equilibrium configuration of cylindrical micro-rods in the single-beam OT geometry [35]. The latter authors found that, for given beam characteristics, a rod can be trapped in different configurations, perpendicular, parallel or oblique, depending on its length and diameter. Rod-shaped particles of micrometer sizes should be trapped parallel to the laser beam axis, which indeed is in line with experimental observations [21,22,36]. Noteworthily the computation of [35] predicts that rods having too large dimensions cannot be trapped by the optical tweezers.

Similarly to rods, optical manipulation of disks poses some difficulties. The problems to be solved may be generalized to oblate ellipsoids or flat-shaped particles in general. Examples of such particles are erythrocytes, fibroplasts, and cells in general. In the technique called "Optical Chromatography" (OC) [37], optical forces are used to separate, concentrate and sort biological species. In addition to shape dependence, orientation of the object and its location within the laser beam critically influences its response to laser illumination. In this context, it is important to get basic knowledge about the optical forces on disks and oblate ellipsoids. Recently Chang *et al.* carried out a numerical work on oblate ellipsoids [38]; the goal was to predict trajectories of such objects in a weakly focused laser beam, of the kind used in OC geometries. Particles, about $8\,\mu$m in diameter were definitely smaller than the beam diameter ($32\,\mu$m at beam waist). The authors computed the trajectories of an oblate ellipsoid as a function of its aspect ratio for different initial locations and orientations. They found that such particles might follow undulating trajectories, but that they would ultimately get laterally trapped along the laser beam axis, in "orthogonal" configuration (*i.e.* with their flat side parallel to the axis). This conclusion is in line with previous observations [39,40] and theoretical determination of equilibrium states [41] of disks or red blood cells in a laser beam (note that Grover *et al.*'s computation took into account the dumbbell-shaped cross section of the erythrocyte). Interestingly, Chang *et al.* noticed that the particle might be either attracted or repelled from the beam axis, depending on its orientation. This property is the source of damped oscillations in the computed particle trajectories.

The above data, either from experiments or numerical simulations may leave the impression that the action of optical forces and torques on rod-, disk-like, or ellipsoidal particles summarize into either stable (immobile) or unstable (rejection from laser beam) states. However, this is not true, because optical forces are fundamentally not conservative [42,43], meaning that they do not derive from a potential function. Because of this non-conservatism, nothing forbids that a particle in a laser beam never comes to rest, but instead moves permanently in a more or less complicated manner. Indeed, a few such situations have been reported. Noteworthily Pauzauskie *et al.* reported that some of their rods would not stay vertically trapped and would undergo sustained back-and-forth tilt motion around the laser beam axis [22]. However no formal interpretation was provided to explain the phenomenon. A similar observation was shortly mentioned by Wilking *et al.*, with the letter I from a colloidal "alphabet soup" [20], with no interpretation either. Neves *et al.* worked with polymeric nano-fibres [21], which they were able to align along the beam axis and stably trap in bulk water. However when the fibre was brought in contact to the cover slip of the sample chamber, it switched to a strongly oblique orientation. In this configuration, the fibre was observed to continuously rotate around the laser axis. Though the authors did not provide an explanation of how the particle would adopt a configuration leading to sustained rotation, they could verify that angular velocities were in line with computed values of optical torques [21].

An observation that may have some similarities with the above-mentioned oscillation of micro-rods [22] has been reported by Cheng *et al.* from trapping experiments with disk-shaped organic particles [40]. The latter authors were able to stably trap disks *in bulk water* over a large range of dimensions (between 0.4 and $20\,\mu$m in diameter) around the focus of a linearly polarized laser [39]. The disks were trapped with their flat sides lying vertical along the beam axis. However, when the optical trap was moved close to the top window of the cell chamber, the disks were observed to undergo sustained oscillations, combining lateral and tilt motions around the beam axis. Cheng *et al.* proposed an interpretation to explain why the disks, which were stably trapped in bulk water, would oscillate when the particle was contacted to the cell top surface. These authors spotted the change in hydrodynamic drag caused by motion along the top surface as the essential difference between both situations. They proposed a model expression for the drag force along the surface that coupled translation and tilt angle of the disk. Based on this expression, they showed that their model would indeed produce a bifurcation, between static and oscillating states [40]. In this model, the control parameter of the bifurcation is the distance z between the beam waist and the top surface.

Our own work, the matter of the following sections, is dedicated to more or less similar phenomena which we observed with ellipsoidal particles, including prolate and oblate shapes. Rather than a tightly focused beam in an optical tweezers configuration, we use a moderately fo-

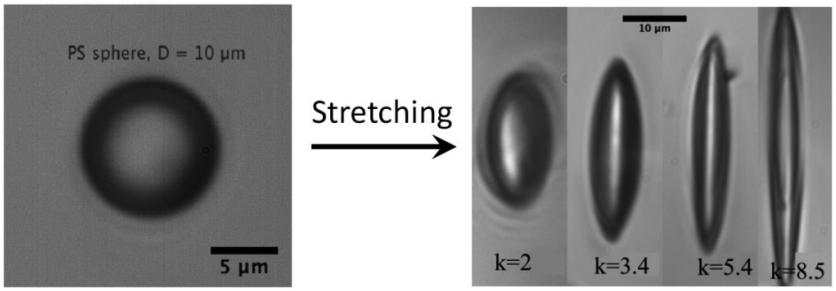

Fig. 1. Examples of prolate ellipsoids made from PS spheres by mechanical stretching. k is the length-to-width ratio of each particle, as seen in the photos.

cused beam in a simple optical levitation scheme. The size parameters of the experiments, and the beam diffraction length l (about $14\,\mu$m), are definitely larger than those involved with micro-rods and single beam traps, but they offer the decisive advantage that the particle can be observed from different directions, while the main physical trends may be extrapolated to the submicron range. Moreover, the ellipsoids have very few birefringence and show little sensitivity to polarization of the laser beam, an appreciable simplification compared to disks and nanoribbons. Experiments show that the ellipsoidal particles either come to rest inside the beam or go through a characteristic back-and-forth motion, with a transition between both regimes that critically depends on the particle aspect ratio. We insist that oscillations occur in general, *be the particle in bulk or close to the top surface*. We offer a systematic experimental characterization of the phenomenon, and propose a physical interpretation based on a simple model of RP forces for an ellipsoid, in 2 dimensions. The model provides a qualitative explanation of why the particles oscillate, essentially because of the structure of optical forces.

This work has been the matter of a recent short publication, whereby we reported key results for elongated (prolate) ellipsoids and a 2-dimensional ray-optics simulation of the ellipsoid-laser beam mechanical interaction [44]. The goal of this full-length article is to provide more detailed experimental observations. We end with a simplified model based on previous simulations that allows understanding the physical origin of the oscillations. The paper is organized as follows:

- In sect. 2, we describe the experimental hardware and procedures. The section includes details on the preparation of the ellipsoidal particles, the levitation setup, and the devices for observation, signal acquisition and recording.
- The main experimental results are presented in sect. 3. Essentially we describe the different behaviors of the particles, in bulk water, close to a fluid-fluid interface and to a fluid-solid interface. Examples are given of periodic and irregular oscillations, depending on particle characteristics. As a major outcome of the observations, a state diagram is proposed that gathers the different dynamic states of particles according to their aspect ratio (k). The diagram includes prolate and oblate ellipsoids, and features the bifurcations between static and oscillating states, with k as a control parameter.
- In sect. 4 we briefly recall the principles of the ray-optics simulation and we examine the structures of the computed optical forces and torques as functions of the particle tilt and off-axis position. Extracting the main features of both functions, we propose a model from which we predict the kind of experimentally observed bifurcation between static and oscillating states.
- The work is summarized in sect. 5, together with prospects for future investigations.

Some more information on technical points is provided as supplementary materials. A detailed description of the procedure used to prepare ellipsoid-shaped particles is given in S1. S2 is about the beam characteristics in our experiments. In S3 we describe a side experiment about the resonance of sub-critical particles and address the problem of the influence of beam polarization on observed dynamics. Details of our multipolar force-torque model are provided in S4.

2 Experimental hardware and methods

2.1 Preparation of anisotropic particles

We used a technique initially designed by Ho *et al.*, and later further developed by Champion *et al.*, to synthesize prolate ellipsoidal particles [45,46]. We used particles made of polystyrene (PS). A detailed description of the preparation method is given in Supplementary Material S1. Briefly, the procedure starts with embedding PS spheres inside an elastic film made of polyvinyl alcohol (PVA). We then heat up the system above the glass transition temperatures T_g of the spheres and slightly below that of the PVA matrix. In the next step, the film is mechanically stretched. The resulting stress deforms the initially spherical particles into approximately ellipsoidal shapes. Uniaxial stretching gives prolate particles, while oblate shapes are obtained by biaxial stretching. Once the PS particles are stretched, the temperature is lowered below T_g. The PS constituent then returns to solid-like state, which allows freezing the particle shape permanently. Ultimately the PVA is removed by washing in water and the

ellipsoidal particles are collected as a dilute water suspension. In our experiments we used spheres $D = 10\,\mu$m in diameter (purchased from either Polysciences, Molecular Probes or Invitrogen). Photos of obtained prolate particles are displayed in fig. 1. The method may be applied to a rather broad range of particle sizes, say from a few hundreds of nanometers up to a few tens of micrometers.

Ultimately we obtain ellipsoids whose shape characteristics are given by a couple of aspect ratios k_1 and k_2: $k_1 = a/b$ and $k_2 = a/c$, where a, b, c are the ellipsoid semi-axes ($a > b > c$, conventionally). In general, we cannot measure a, b, c separately from simple microscope views, as in fig. 1, because each particle can be observed only from the top (meaning only one direction). Fortunately the 3-dimensional particle shape can be observed in the levitation experiments, when the particle is lifted up with its long axis vertically oriented. We are thus able to determine a, b, c separately, and then $k_{1,2}$ with a $\pm 2.5\%$ relative uncertainty. Based on this procedure, we discovered that the stretching procedure does not yield axisymmetric particles (otherwise called "spheroids") in general (meaning $a \neq b \neq c$). Nevertheless, a small fraction of the population is found to be approximately symmetric, *i.e.* $b \approx c$, within a 10% uncertainty.

2.2 Optical setup

The core of the setup is sketched in fig. 2a. Optical levitation of individual particles is achieved by means of a green Gaussian laser beam ($\lambda = 514\,$nm, from an argon ion laser in the early versions of the setup, now from a solid state Coherent Genesis laser). The beam is made vertical ($\parallel z$) by reflection on the dichroic mirror DM, and focused through ML_1 objective inside the glass cell (GC) that contains the particles. The part of the setup upstream of DM is sketched in fig. 2b. L_1, L_2, L_3 objectives play the same roles as in classical optical tweezers designs (see, *e.g.*, [47]) based on Keplerian telescopes. Lens L_1 focuses the beam on a couple of closely assembled galvanometric mirrors (GM), whose position is conjugate to that of ML_1 rear focus through L_2 and L_3. Rotating each of GM mirrors then results in horizontally translating the beam inside the sample volume.

The beamwaist radius in GC (ω_0) may be varied between 9 and 1.25 μm, essentially by changing the distance between L_1 and L_2 (see Supplementary Material S2 for details). In this paper, we report data that were obtained with $\omega_0 = 1.3\,\mu$m. We measured a beam diffraction parameter $M^2 \approx 1.14$ indicating that the laser has a good beam quality. The beam diffraction (Rayleigh) length is about $14\,\mu$m.

A couple of digital cameras (C_1, C_2) yield simultaneous video images of the particle, from top through ML_3 and laterally through ML_2, with a $\times 50$ magnification. ML_1, ML_3 (Zeiss) and ML_2 (Mitutoyo) are long-working distance microscope objectives. The top view may be focused into the plane of beam waist ($z = 0$) or at finite distance from it ($z > 0$ or < 0). We can vary z between about -100 and $+100\,\mu$m. Observing levitated particles from both top and side is made possible using parallelepiped cells that have polished sides in all directions. Ours (from Thuet, France) are 1 or 2 mm in thickness.

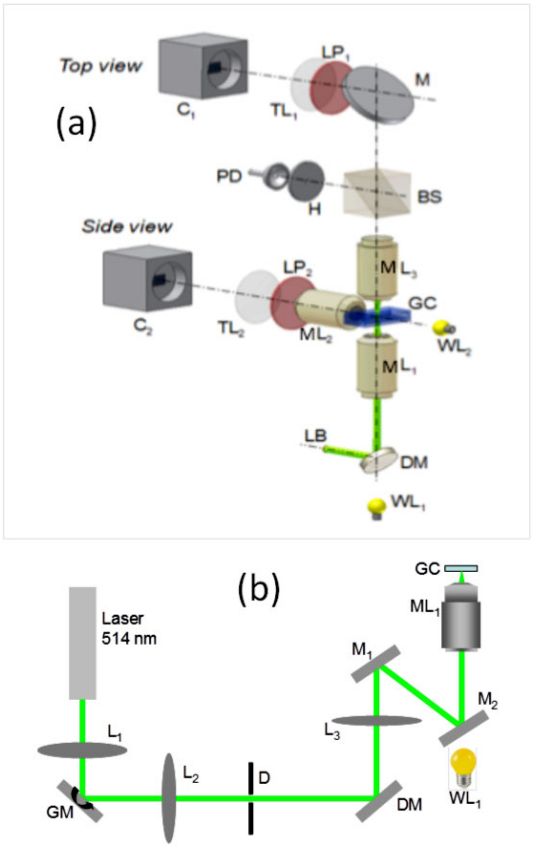

Fig. 2. (a) Sketch of optical setup. (b) Upstream part of the setup, used for beam shaping and translation. The elements are not to scale, for clarity. LB: laser beam. BS: beam splitter. $TL_{1,2}$: tube lenses. $LP_{1,2}$: long-pass (red) filters. $M_{1,2}$: mirrors (max. reflection at 22.5° incidence at 514 nm). D: diaphragm. Bright field illumination is provided by two white light sources ($WL_{1,2}$), in Koehler configuration. See text for other symbols definitions.

A typical experiment starts with capturing one particle from the suspension. As the PS has a density ($1.05\,\mathrm{g/cm^3}$) slightly larger than that of water, most of the particles are found lying on the lower boundary of the chamber, with a little but discernable amount of Brownian motion. A simple method amounts to horizontally shifting the cuvette to bring a particle across the laser beam. Figures 3a,b illustrate the procedure in the simple case of a spherical particle. The laser beam then drives levitation; the sphere locks onto the beam axis and starts lifting up. The ascension ends when the particle gets in contact to the chamber's top surface (fig. 3b). Interestingly, ascension may be stopped somewhere in bulk water, away from glass boundaries, if one tunes the laser power to a small value P_{lev} (2 mW is typical), just enough to equilibrate the particle's buoyant weight. Optical trapping of a sphere is not really achieved in optical levitation with a single beam, because the vertical equilibrium is not stable. Strictly speaking, the moderately focused laser beam

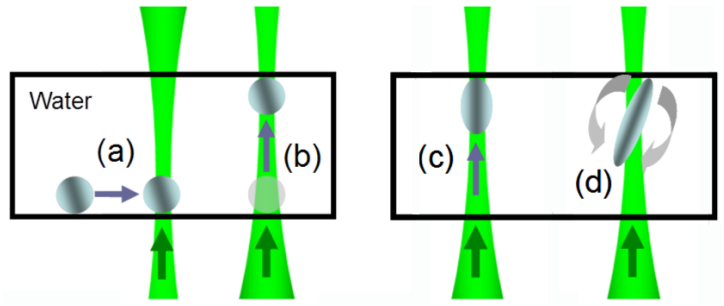

Fig. 3. General sketch of optical levitation experiments. The figure illustrates the case when the laser beam waist and the observation plane coincide, *i.e.* $z = 0$. The black frame represents the boundaries of the sample glass cell. (a,b): Levitation of a spherical PS particle. (c,d): Levitation of a short prolate ellipsoid (c), and of a large-aspect-ratio ellipsoid (d). In the latter case, the particle oscillates in the laser beam, in bulk water and in contact to the cell top wall.

only provides 2-dimensional (x, y) trapping. However, it is possible to tune the power such that the particle hardly drifts up or down within about a minute, allowing for a precise determination of $P_{\rm lev}$. Real 3-dimensional equilibrium is achieved when the sphere hits the ceiling of the cuvette (fig. 3b), as the particle gets locked by the optical forces and the contact force exerted by the glass surface. The sphere there is kept immobile (fig. 3b).

The steps to start levitation of ellipsoids are the same as for a sphere (figs. 3c,d) with the capture of a particle lying at the bottom of the cuvette. Levitation of a short ellipsoid ($k < 3$, say) is very simple and technically similar to that of a simple sphere. We start the experiment by picking up one ellipsoidal particle with the laser. Within a few seconds, the particle stands up and starts levitating. Levitation ends with the ellipsoid sitting vertically in contact to the cuvette ceiling, as sketched in fig. 3c. Levitation of longer ellipsoids is more delicate, because these particles do not keep locked on the laser beam axis and constantly oscillate, moving out and back to the axis. Lifting the particle up to the top demands frequent feedback from the experimentalist, using the x, y translation stages to keep the particle within the beam. Very small aspect ratio ellipsoids, meaning rather flat disk-like particles, behave similarly to elongated ellipsoids, as they constantly oscillate.

2.3 Data acquisition and analysis

We characterized particle dynamics directly from video images or indirectly from the 1-dimensional signal of a photodiode.

2.3.1 Photodiode signal

The photodiode (PD in fig. 2) records the transmitted laser power through a pinhole (H). The photodiode signal $I(t)$ thus bears direct information about the optical loss due to scattering of light by the particle. An oscillatory motion results in time modulation of $I(t)$. By nature and contrary to video movies, $I(t)$ is a global signal, from which it is not possible to unravel translation and rotation components of the particle's motion. However the photodiode signal offers the advantage of high resolution in time, with sampling frequencies up to 10 kHz, much higher than video frame rate.

2.3.2 Video and particle tracking

Images and movies are acquired from the two CCD cameras (Edmund optics) simultaneously using StreamPix software. This enables us to observe the system from different directions, with a frame rate up to 40 Hz. The recorded images are used to determine particle size, aspect ratio and beam position. Position and tilt angle of a particle are determined through a particle tracking procedure. We use a home-made autocorrelation treatment that comes as a plugin of ImageJ software (NIH Image). At the current stage, the analysis is based on the assumption that the ellipsoidal particle is axi-symmetrical (*i.e.* a spheroid). In this context, and neglecting the influence of beam polarization (see Supplementary Material S3), the orientation of the oscillation plane around the laser beam axis is degenerate; then only one coordinate (θ) is necessary to define the particle angular configuration. In spite of the above limitation, the procedure is applied even to non-symmetrical particles. In the latter case, θ plays the role of an effective tilt angle, in reality a function of the particle's three Euler angles.

For each video frame, the analysis yields an elliptical contour that best fits to the image of the particle. The procedure is illustrated in fig. 4 with a sequence of consecutive side view images of an oscillating particle. The uncertainty in θ is $\pm 0.8°$ (see table 1).

Note that the side view only yields an apparent tilt $\theta_{\rm tilt}$ ($< \theta$) that is equal to θ only when the plane of oscillation $\Pi_{\rm osc}$ is perpendicular to the axis of the side camera (this is so in fig. 4). The particle tilt may be obtained from top views as well, without any restrictive condition on the orientation of $\Pi_{\rm osc}$. However the accuracy of the latter method becomes poor for small values of θ. The optimum performance is obtained by combining top and side observations, using top views to monitor the orientation of $\Pi_{\rm osc}$ and side views to measure θ.

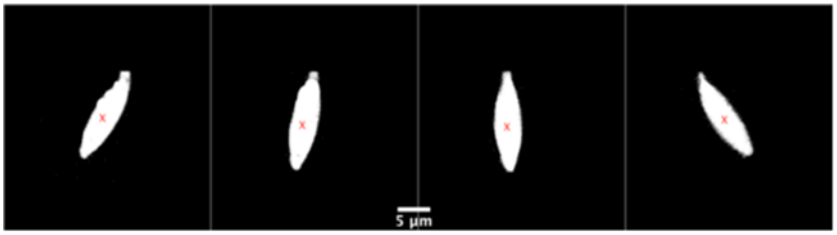

Fig. 4. Analysis of consecutive images of an oscillating ellipsoid from side view movie.

Table 1. Output file from particle tracking, in correspondence to the frames of fig. 4. The origin of the tilt angle ($\theta = 0$) is taken for the particle symmetry axis lying vertical (parallel to the laser beam axis).

Time [s]	x [μm] ± 0.5	y [μm] ± 0.5	θ [deg] ± 0.8
0	2.7	−1.7	27.2
0.1	0.5	1.1	10.7
0.2	−0.2	0.5	−2.2
0.3	−3	−0.8	−33.5

2.3.3 Analysis of oscillations

In many examples (see sect. 3), recorded signals turned out periodic, within experimental noise: this was most evident from video records analysis, which showed simple closed trajectories in (x, y, θ) space. The corresponding photodiode signal was analyzed using standard Fourier decomposition, yielding well-marked peaks at fundamental and harmonic frequencies in the power spectra.

Reported data in this article are limited to time series and corresponding Fourier spectra. In the case of non-periodic signals, Fourier analysis was complemented by phase space reconstruction analysis (see, *e.g.*, [48]), as is commonly used in non-linear dynamics problems. The goal of this analysis was to reveal cases of deterministic chaos in certain types of signals whose power spectra did not show any well-marked frequencies. This part of the work, being currently under investigation, is beyond the scope of this article; results will be the matter of a later report.

3 Oscillating particles—experimental observations

In this section, we first report observations of particles in bulk water, in a pure levitation scheme, meaning that the laser is operated at small power (3 mW, typically), just enough to sustain the weight of the particle. Next we turn to the case of particles pushed up to contact with the upper boundary of the sample cell, which may be a water-air, water-oil or simply the water-glass interface. In the latter configuration, the laser power may be increased at will, since the particle's altitude is bounded by the interface.

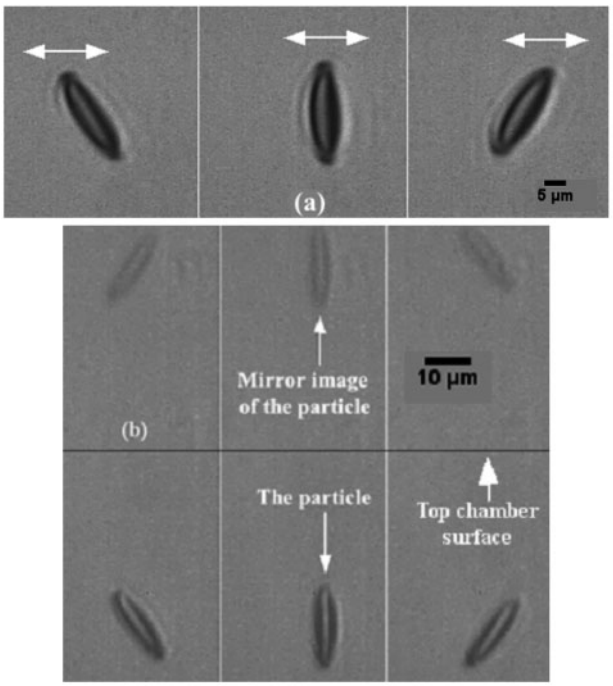

Fig. 5. Lateral view of an oscillating prolate ellipsoid. (a) In bulk, far away from the surfaces, where the mirror image of the particle is out of the view of the camera. The arrows show the oscillation direction. (b) Near the top surface, where both the particle and its mirror image are visible. The bottom one is the true particle located few microns below the black straight line (approximate location of the top chamber surface). Images were recorded every 1 second.

3.1 Particle behavior in bulk water

Optical levitation of a spherical PS particle in water is a straightforward experiment that allows keeping the particle at about constant altitude in bulk fluid, anywhere inside the sample cell. In a similar experiment with non-spherical particles, we observed that such particles, either come to rest inside the beam or go through a characteristic dancing motion, with a transition between both regimes that critically depends on their aspect ratio. With prolate ellipsoids, of average aspect ratio k, oscillation appears when k is larger than a threshold value ($k > k_{\mathrm{CP}}$, where the index P stands for "prolate"); see fig. 5. Similarly, an oblate particle oscillates if it is flat enough, *i.e.* if $k < k_{\mathrm{CO}}$

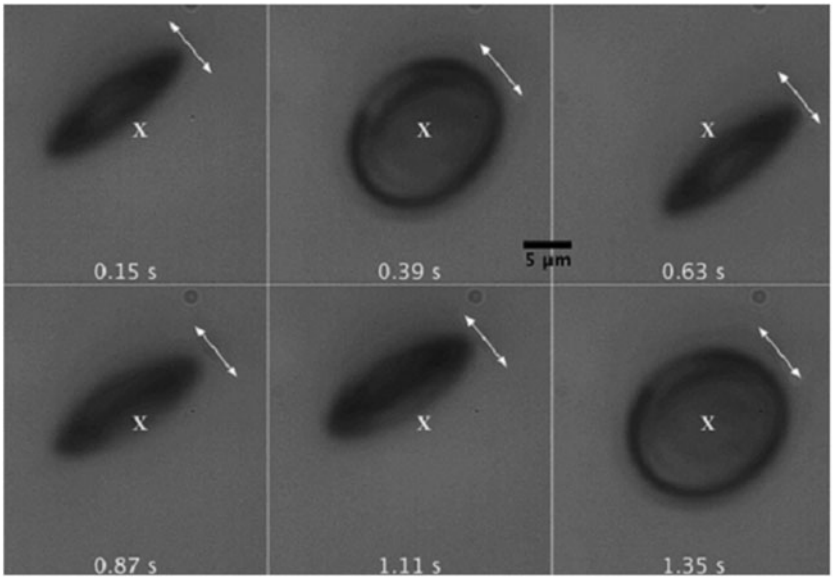

Fig. 6. Top view of an oscillating oblate ellipsoid in bulk water. The white cross "X" locates the position of the beam center. The arrows represent the oscillation direction.

(index O stands for "oblate"); see fig. 6. In such cases, the particle is seen to oscillate as soon as it comes into the laser beam, at the beginning of the experiment and during ascension. We thus bring the particle up in bulk water, away from the cell bottom and still well below the cell ceiling. By tuning the laser beam power down to an appropriate value, of the order of 3 mW, we are able to cancel ascension and maintain the particle at about constant altitude. There, it undergoes sustained oscillations, combining angular and translational excursions (both laterally and in altitude).

Figure 5 shows lateral views (captured by camera C_2, see fig. 2a) of an oscillating prolate particle, deep in bulk water (fig. 5a) and at short distance (Δh) from the top water-glass interface (fig. 5b). As the interface is highly reflective at grazing incidence, a mirror image of the particle is visible on top of the images. The distance between the tips of the particle and its image is simply $2\Delta h$.

3.2 Particle in contact to an interface, at the beam waist (z = 0)

In spite of their formal simplicity, experiments in bulk water are delicate for they require the use of very low laser power, resulting in slow particle motion, with a unique frequency determined by the levitation power. Therefore, for practical convenience, most of our experiments were carried out with the particle touching the upper interface of the sample cell. Contact to the interface serves as a condition to fix the altitude of the particle below an upper boundary, and, most interestingly, allows the experimenter to vary the laser power at will. As we will see, having the particle in contact to the interface rather than in bulk brings no change to the observed oscillatory motions, at least qualitatively.

3.2.1 Fluid-fluid interface

We start with the case of a water-oil (W/O) interface. We matched the viscosity of the oil to that of water ($\eta = 1$ mPa s at room T). Matching was achieved using a decane:undecane mixture (79.5 : 20.5%wt), as in [49]. Surface tension is large enough to maintain a flat interface, even when the particle is pushed up by the optical levitation force. Compared to bulk water, the water-oil interface essentially imposes a zero vertical velocity component ($v_z = 0$) of the fluid at the altitude ($z_{\rm int}$) of the interface. The condition is then intermediate between bulk water and a solid interface (where v_x, v_y, $v_z = 0$ at $z_{\rm int}$).

Very similarly to behaviors in bulk water, short prolate ellipsoids did not oscillate, while longer ones did; see the example shown in fig. 7a. Thus the bounding condition in z turns out not essential for the existence of oscillations.

The case of water-air interface, intermediate between water-oil and water-glass, does not differ from the general tendency; see the example of an oscillating oblate ellipsoid in fig. 7b. As we mentioned above, only the tip of the particle is in contact with the interface, meaning that the particle body is entirely inside water (a kind of complete wetting). This is strictly true with the water-glass interface. In the case of water-air or water-oil interface, complete wetting is maintained only for a while, from a few seconds up to several minutes, say. This leaves enough time for oscillations to be observed and recorded, as reported above. Ultimately, the particle gets through the interface and settles in a partial-wetting configuration, which is energetically favorable. The transition from complete to partial wetting is irreversible, and is a dynamically complex phenomenon [50].

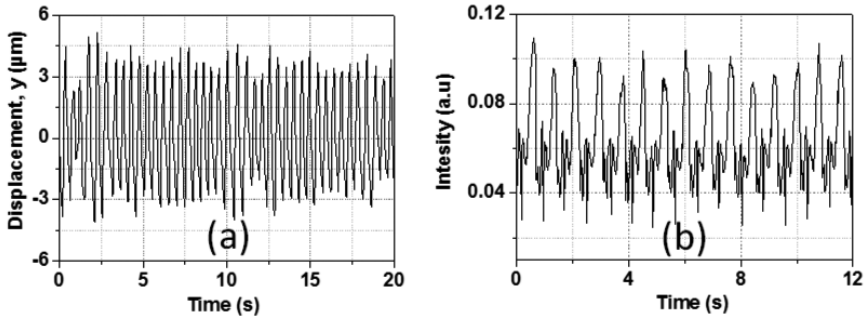

Fig. 7. (a) Horizontal motion (y coordinate) of an oscillating prolate ellipsoid ($k_1 = 4.1$, $k_2 = 3.8$) in contact to a water-oil interface. $P \simeq 15\,\mathrm{mW}$ and $z = 0$. (b) Photodiode signal from an oblate ellipsoid ($k_1 = 0.26$, $k_2 = 0.3$) oscillating in contact to a water-air interface. $P \simeq 15\,\mathrm{mW}$ and $z = 0$.

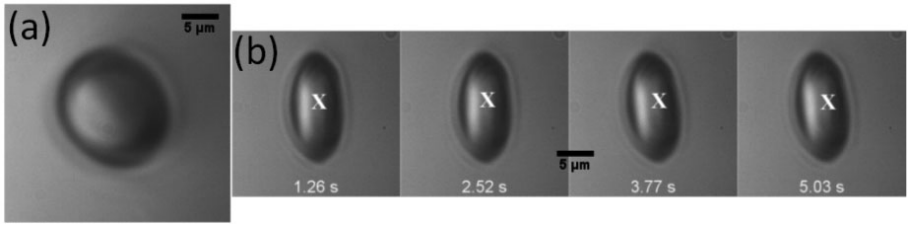

Fig. 8. Static configuration of an oblate ellipsoid of moderate ellipticity ($k_1 = 0.48$, $k_2 = 0.44$). (a) Particle lying on the cell floor before laser illumination. (b) The laser locks the particle with its flattened side vertical. The white cross "X" represents the beam position. The numbers at bottom indicate the time seconds.

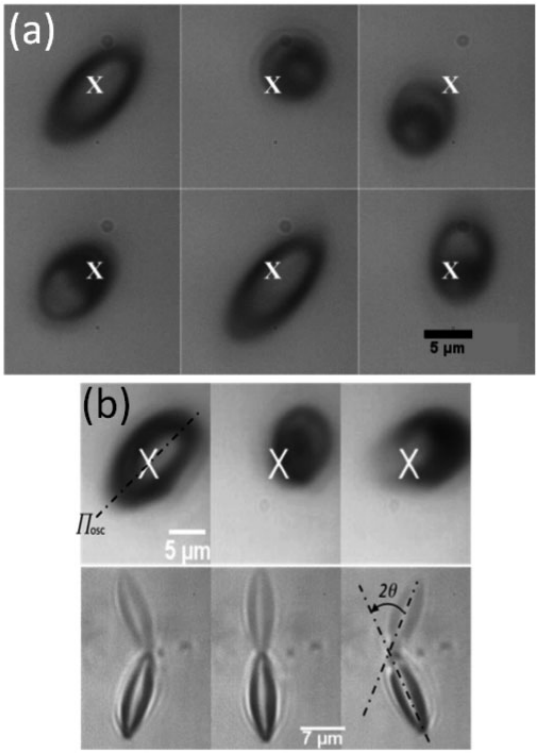

Fig. 9. (a) Large-aspect-ratio ellipsoid (top views): Consecutive images taken every 0.1 second showing different positions and orientations in time. The white cross represents the location of beam axis. (b) Combined top and lateral views. Photos in the upper row are top views (xy plane), and those in the lower row are side views (xz plane). Successive frames are separated by 0.1 second. The dot-dashed line in the top marks the instantaneous plane of oscillation (Π_{osc}). The angle indicated at the bottom (2θ) is twice the particle long axis tilt angle. Aspect ratio of the ellipsoid: $k_1 = 3.6$ and $k_2 = 3.3$.

3.2.2 Water-glass interface

We now turn to the case of a water-glass interface, by far the most exploited configuration in our experiments. Compared to fluid interfaces, a glass wall introduces a no slip condition, meaning that the fluid velocity has to be zero at the solid surface. While this condition makes the hydrodynamic drag of the particle different from that in bulk or with fluid interfaces, experiments indicate that major trends in particle dynamics (essentially the bifurcations between static and oscillating states) are the same whatever the nature of the interface.

We shall present the different types of particle dynamics, according to particle shape parameters. Recall that this subsection only deals with the case of a particle located close to the beam waist plane ($z = 0$). Cases of particles away from the beam waist plane (meaning $|z| > l$) are the matter of subsect. 3.3.

Static equilibriums are observed with particles of "moderate ellipticity", namely prolate particles of $k < 3$ or oblate ones of $k > 0.33$. A prolate spheroid locks on the laser beam with its symmetry axis vertical. A slightly oblate particle (see fig. 8) gets immobilized too, but with its symmetry axis lying horizontal. Strictly speaking, the above statements only hold for symmetrical particles ($k_1 = k_2 = k$), but the rule still roughly applies to non-symmetrical particles that are not far from axisymmetry (as is the case in fig. 8).

Sustained oscillations are systematically observed with particles of large ellipticity ($k > 3$ or $k < 0.33$). An oscillating particle executes a kind of "dance", consisting in back and forth motions both in position and orientation; see the example of a prolate particle in fig. 9.

Whether the motion is periodic or not depends on the particle shape parameters and its position along the beam

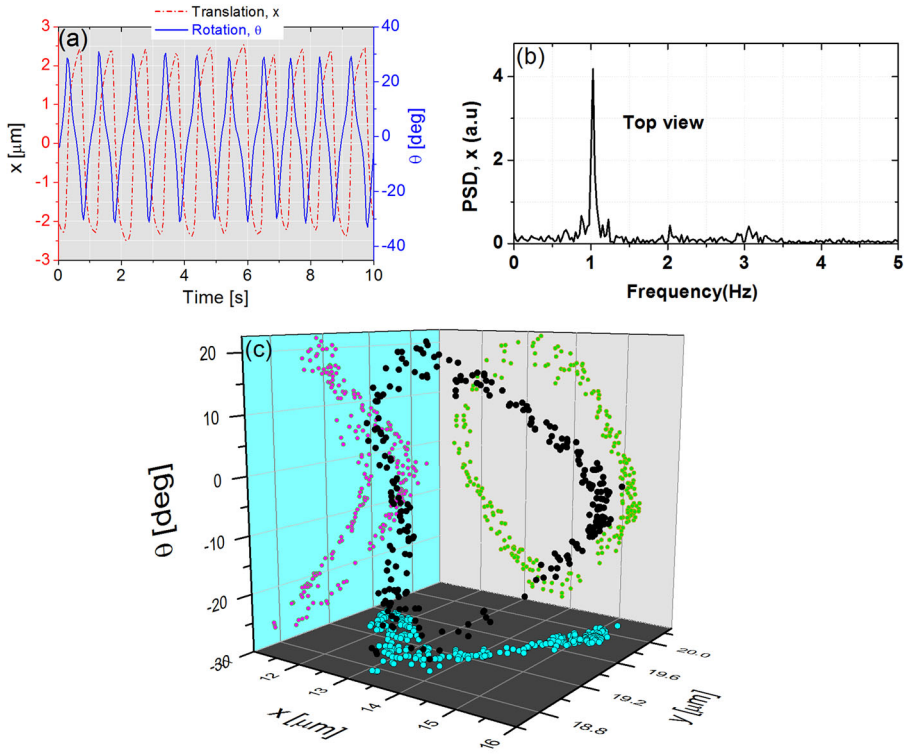

Fig. 10. Particle aspect ratio: $k = 4.5$; data obtained from video images. (a) Black curve: particle horizontal x-translation. Blue curve: particle tilt (θ). (b) The power spectral density of the particle horizontal motion (x). (c) $2d$ projections (colored symbols) of the corresponding $3d$ trajectory (black symbols) in phase space showing a limit cycle. Oscillation frequency is close to 1 Hz at a laser power of 11 mW.

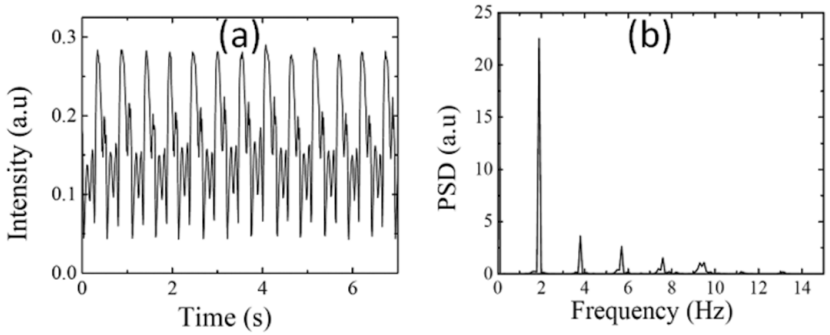

Fig. 11. Data recorded with a ($k_1 = k_2 = 3.8$) particle. (a) Modulation of the on-axis laser power recorded with the photodiode and (b) corresponding power spectrum density; fundamental frequency ≈ 2 Hz. Laser power: 19 mW.

axis. It is not completely clear to us to identify the required conditions for the motion to be periodic (or not). However, we frequently observed that periodic oscillations were obtained with ellipsoids that were close to symmetrical ($k_1 \cong k_2$) and of moderate aspect ratio ($k < 5$, say, in $z = 0$ configuration). An example pertaining to this category is shown in fig. 10. Data in fig. 10 have been obtained by video image analysis, which yielded translational and rotational coordinates of the particle in time. The periodicity of the motion is illustrated by the well-marked peak in the power spectrum of the x-coordinate (fig. 10b) and by the limit cycle in the (x, y, θ) representation. Another example of a presumably periodic motion, based on the photodiode signal, and the associated Fourier power spectrum, is shown in fig. 11.

The period —more generally the characteristic time— of the oscillations is directly controlled by the laser power. Increasing P decreases the period. We observed that the frequency (f) of oscillation of PS ellipsoids just scales linearly with the laser power. This result is similar to that previously reported by Cheng *et al.* [39,40] for birefringent wax disks. Changing the power does not change the

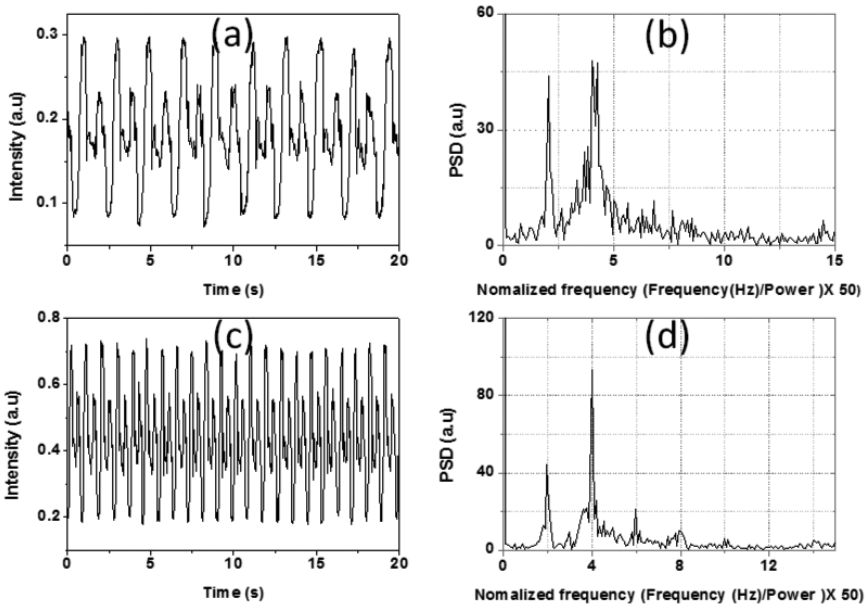

Fig. 12. Photodiode signal from an oscillating particle ($k = 4.1$) at two different powers. (a,c): Time series at 9.1 mW and 22.3 mW, respectively. (b,d): Corresponding power spectral densities (PSD). For clarity, the frequency has been normalized by the laser power.

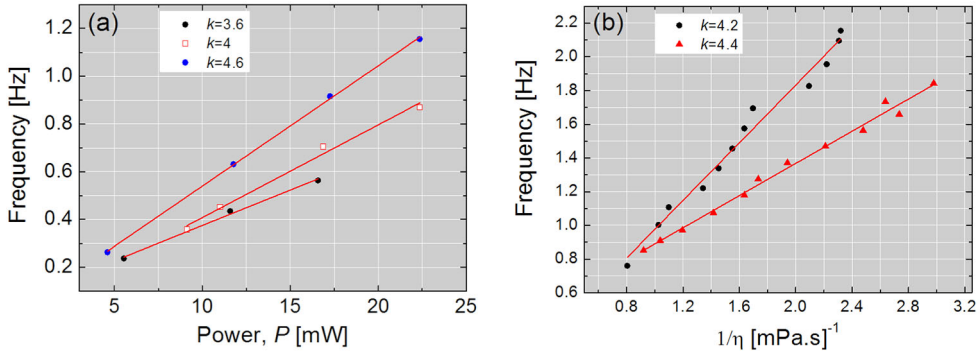

Fig. 13. Proportionality of the oscillation characteristic time to η/P. Dependence on laser power (a) and fluid viscosity (b), measured with different prolate particles.

dynamical state qualitatively, see fig. 12 for illustration. Within experimental noise, the signal keeps the same morphology, while the time scale is divided by 2.44, the ratio of involved powers. We repeated the same test for different particles and reached the same conclusion, see fig. 13a for a summarizing graph.

The proportionality of f to P is what we expect based on the simple principle that the particle motion is driven by optical forces, proportional to P, balanced by Stokes drag forces, proportional to the fluid viscosity (η). We then guess that f is inversely proportional to η. We verified the latter dependence experimentally by varying the temperature of the water from 10 to 60 °C, resulting in a viscosity change from 1.2 to 0.3 mPa s (a three-fold decrease of the viscosity). As the corresponding change in index of refraction is insignificant ($< 0.5\%$), the optical forces are about constant. The temperature was regulated by circulating water and a thermocouple was used to measure the temperature of the water medium inside the sample cell. We measured the oscillation frequencies of a few ellipsoids as a function of the sample temperature. We found a linear relationship between viscosity of the medium and period of oscillation, within statistical scatter (fig. 13b).

These tests show that the P/η ratio intervenes as a scale factor of the time variable. Experiments indicate that the laser power has about no influence on the *amplitude* of oscillations. This can be seen from fig. 12a,c, showing the fluctuations of the photodiode signal (I) for two different values of P. Oscillations in I around the mean value, namely $\Delta I = I - \langle I \rangle$, are the signature of particle oscillations. Because the photodiode is a linear detector, $\langle I \rangle$ and ΔI are proportional to P. In experiments, the amplitude of oscillation (given by (x, θ) variables in a $2d$ representation, see sect. 4) is represented by $\Delta I/P$.

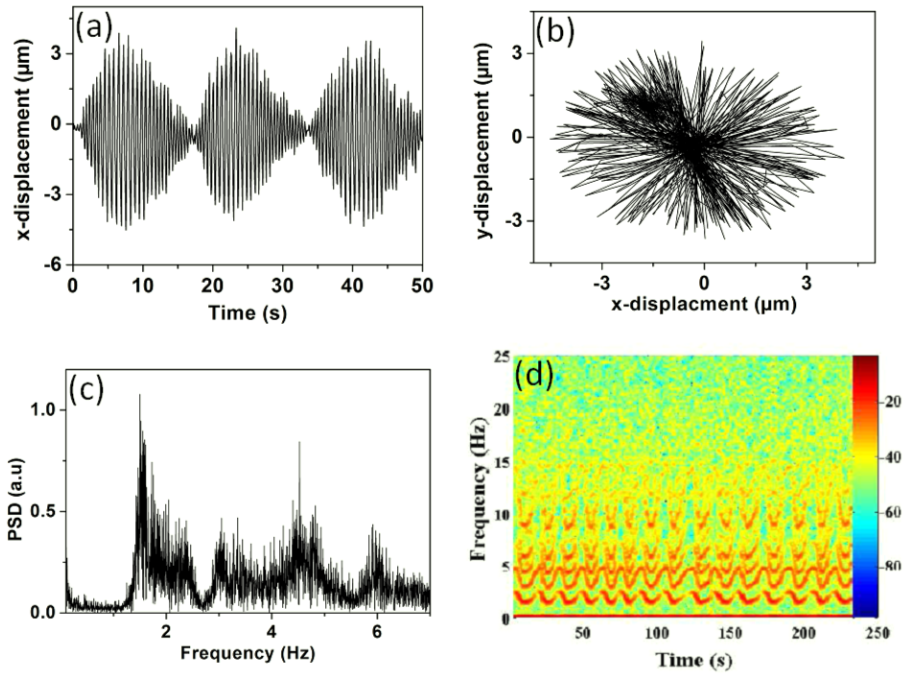

Fig. 14. Example of non-periodic dynamics. Aspect ratio: $k_1 = 4.2$, $k_2 = 4$. (a,b): data from video analysis. (c,d): data from photodiode signal analysis (see text for details).

As can be read from fig. 12, $\Delta I/P \approx 0.022$ for $P = 9.1$ and 22.3 mW, indicating that particle excursions were the same for both powers. Though this conclusion may seem at odd with intuition, it is in line with the model presented in sect. 4.

In contrast to axi-symmetric moderately elliptical particles, non-symmetrical and/or longer particles gave non-periodic or irregular signals, with no well-marked peaks in the frequency spectrum. On fig. 14 we show the example of a particle having $k_1 = 4.2 \pm 0.05$ and $k_2 = 4.0 \pm 0.05$. Main features, gathered from video image analysis, are: i) The amplitude of oscillations is modulated in time, see fig. 14a, and ii) the plane of oscillation ($\Pi_{\rm osc}$, defined as in fig. 9) rotates continuously, see fig. 14b. Recorded time series reveal that the motion combines amplitude and frequency modulations. The frequency modulation is visible in the diagram of fig. 14d, which was obtained from a time-frequency analysis of the photodiode signal [51]. The modulation looks periodic, with the same period as the amplitude modulation, about 16 s.

The above example still has a rather simple structure, which we tentatively described in terms of combined amplitude and frequency modulation. We carried out many more observations with a variety of elongated non-symmetrical particles, and obtained a whole wealth of complex oscillation dynamics, with no clear underlying structure.

We end this subsection by gathering the information on particle dynamics into a *state diagram*. The diagram (fig. 15) summarizes the dependence of the dynamical state on particle shape parameters. We specify only k_1 and k_2 as control parameters, since the laser power is not essential. Note that the displayed diagram only holds for ellipsoids whose centers are about in the beam waist plane ($z = 0$). The top right quarter corresponds to prolate ellipsoids. Increasing $k_{1,2}$ indicates particles which are more and more elongated. Points close to the diagonal mean that particles are about cylindrically symmetrical, while those well outside of the diagonal are far from symmetrical. The bottom left quarter corresponds to oblate ellipsoids. In this case, small $k_{1,2}$ values refer to flattened particles. The diagram allows to classify particles into static and oscillating, with two bifurcations ($k_{\rm CP} \cong 3$ and $k_{\rm CO} \cong 0.33$) in between, on the prolate and oblate sides, respectively. Solid red circles correspond to particles which are stably trapped by the laser beam. In this class, nearly symmetrical particles simply do not move (apart from very small Brownian fluctuations), and stay in on-axis configuration. Solid white circles correspond to sustained "dance", of which we gave examples above. Solid blue squares correspond to what may be termed "sub-critical" particles, meaning ellipsoids whose aspect ratio is only slightly less than $k_{\rm CP}$ or slightly larger than $k_{\rm CO}$. Such particles are within the bifurcation threshold and then do not permanently oscillate, but they are very "susceptible": when such a particle is slightly pushed away from the beam axis in x or y, it comes back to vertical equilibrium through a few damped oscillation cycles. Interestingly, oscillation of a subcritical particle can be excited by back-and-forth shift of the laser position (see Supplementary Material S3). The excitation can be made resonant by matching the frequency of the laser beam lateral shift to that of the particle.

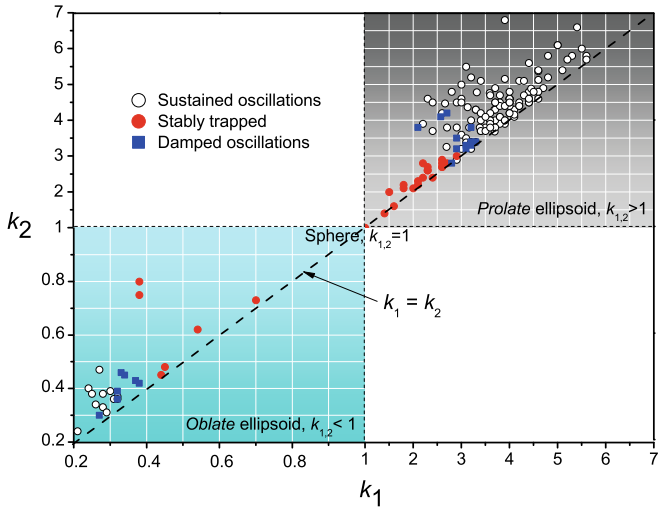

Fig. 15. State diagram, summarizing the dependence of the dynamical state on particle shape parameters $k_1 = a/b$ and $k_2 = a/c$ (see sect. 2.1). All data of the diagram correspond to $z = 0$, *i.e.* particle centers were approximately at the altitude of the laser beam waist.

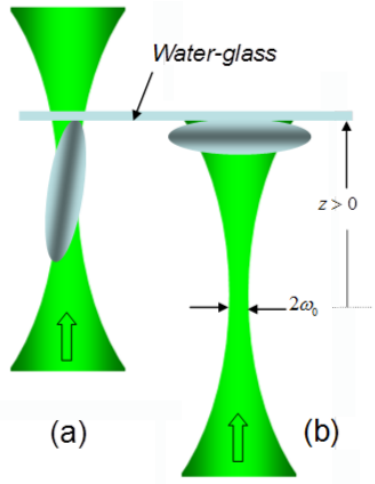

Fig. 16. (a) Ellipsoidal particle located at the beam waist. In average, the long axis of the particle is aligned parallel to the beam axis. (b): The same particle, when far enough from the beam waist, switches to horizontal static equilibrium.

3.3 Influence of beam diameter and wave curvature

Up to now we only considered particles whose centers were close to the beam waist ($\omega_0 = 1.3\,\mu$m), at $z = 0$, by definition. Now we want to estimate the influence of changing the axial position of the particle. In our experiments, the particle is in contact to the glass cell top surface, and observation is focused in this plane. We vary z by shifting the laser beam waist vertically to a position either below (then $z > 0$) or above ($z < 0$) the observation plane. By changing z we vary both the beam diameter ($2\omega(z)$) and the wavefront curvature felt by the particle; see fig. 16. The beam width increases with $|z|$, while the wave is convergent for $z < 0$ and divergent for $z > 0$. The reference length to estimate the amplitude of the change in z is the beam diffraction length, $l = \pi\omega_0^2/\lambda$. With $\lambda = 386\,$nm for the laser wavelength in water, l is about $14\,\mu$m. The beam diameter is twice that of the beam waist ($2\omega(z) = 4\omega_0^2 \cong 5.4\,\mu$m) for $z = \sqrt{3}l \cong 24\,\mu$m.

In what follows, we only consider prolate ellipsoids, which are long enough to oscillate at $z = 0$. As a general trend, we observe that a moderate increase in $|z|$, on the order of l, does not suppress the oscillations, but it does change details of the dynamics. Conversely, oscillations are "killed" at large l, when the beam width becomes comparable to the particle (large) size. In this case, the particle switches to static horizontal equilibrium, as sketched in fig. 16b. The impact of a small change in l is illustrated below, with two examples. We observed that increasing the beam width may change the particle dynamics from irregular to approximately periodic (fig. 17) or in the opposite way (fig. 18). Figure 17 refers to a particle that was oscillating in a complicated manner at $z = 0$, with combined motions in x, y, θ and in the orientation of the oscillation plane. The irregular dynamics recorded at the beam waist changed to more regular dynamics when the particle was located upstream of the beam waist ($z < 0$) plane, with a concomitant stabilization of the oscillation plane.

The example displayed in fig. 18 shows the opposite trend, now with a particle whose oscillatory motion was periodic at $z = 0$, and which became irregular for negative z. We made similar observations with particles at $z > 0$, confirming that both types of changes (periodic $\leftrightarrows$ irregular) were possible on both sides of the beam waist plane.

A vertical-to-horizontal (V-to-H) transition occurs at large $|z|$, when the beam diameter becomes very large. The transition is illustrated below (fig. 19). The photos are top views, showing an elongated particle ($k \approx 4.9$). z was initially tuned to $z_i \approx 50\,\mu$m, a configuration where the particle was permanently oscillating. The sequence shows the response of the particle dynamics to an increase in z, up to $z_f \approx 80\,\mu$m. The particle still goes through a few slow oscillations (top row) and then comes to rest in horizontal equilibrium (bottom row). We shortly investigated the influence of beam polarization on the particle horizontal equilibrium. The conclusion is similar to that drawn for oscillating states, *i.e.* we did not notice any clear correlation. H configurations of prolate ellipsoids were randomly oriented.

The V-to-H transition, *i.e.* the change in orientation of spheroids from vertical (either statically or in average) to static horizontal alignment in response to increasing beam width, holds for both oscillating and non-oscillating prolate ellipsoids. But the transition value of z ($= z_{\rm VH}$) which causes the particle to flip horizontal, varies from particle to particle. As a rough indication, we observed that the transition occurred when the beam diameter $2\omega(z_{\rm VH})$ was between 60% and 80% of the particle length ($2a$).

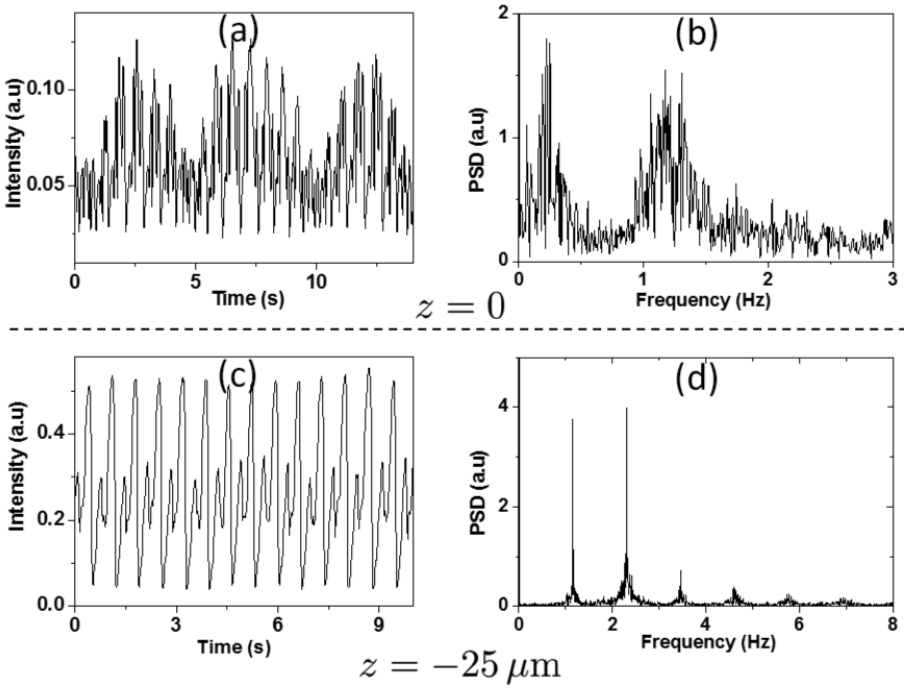

Fig. 17. Non-symmetrical ellipsoid ($k_1 = 4$, $k_2 = 3.6$). In (c,d) the particle is located upstream of the beam waist plane. (a,c): Time series signal from photodiode. (b,d): Corresponding Fourier power spectrum density.

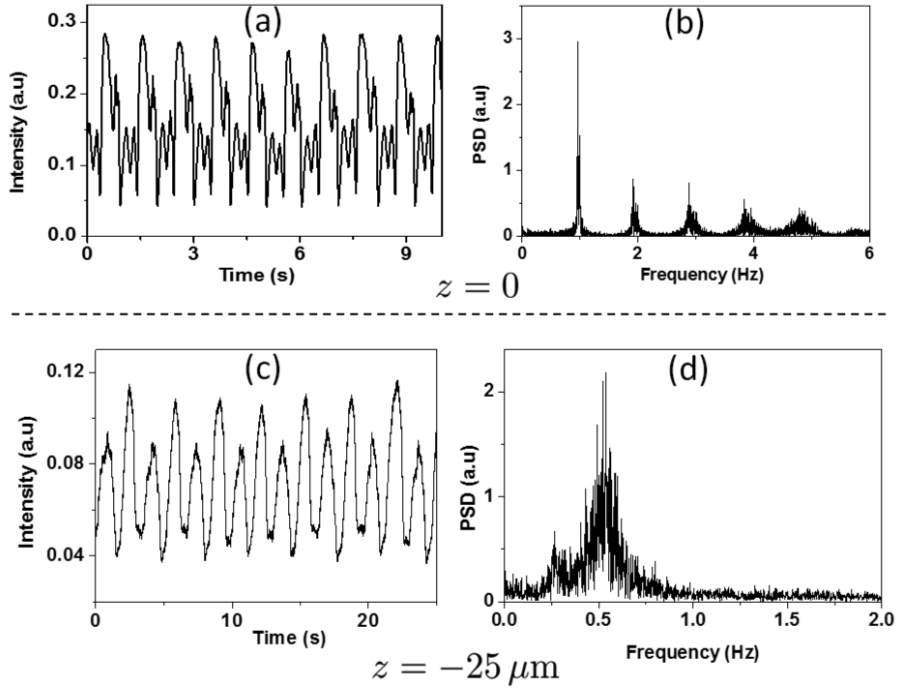

Fig. 18. Symmetrical ellipsoid ($k = 4$). In (c,d) the particle is located upstream of the beam waist plane. (a,c): Time series signal from photodiode. (b,d): Corresponding Fourier power spectrum density.

Summarizing:

Whatever the type or shape of the particle, oscillations of prolate ellipsoidal particles disappear for large enough beam width. Thus, the necessary conditions for the oscillations to exist are:

- the particle should be elongated enough ($k > 3$),
- the beam width should not be too large ($z < |z_{\max}| = z_{\mathrm{VH}}$)

whereas the type of dynamics is controlled by:

- the symmetry and aspect ratio of the particle,
- the beam width.

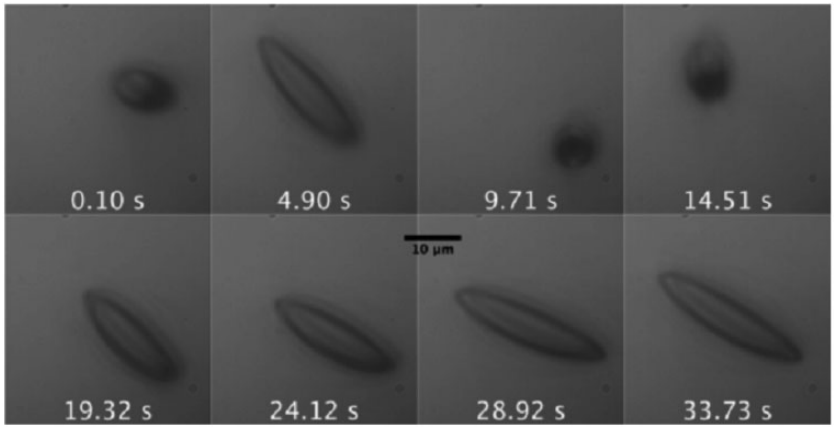

Fig. 19. Video images of a prolate ellipsoid showing the transition to horizontal orientation. Once the particle is lying flat on the interface, it does not show any form of sustained oscillation.

4 2d simulation and 4-pole force/2-pole torque model

In [44] we proposed a minimal description of the mechanical effect of the laser beam on ellipsoidal particles using the ray-optics approximation. The simulation is restricted to dimension 2; meaning that light rays are confined inside a vertical plane and the particle is reduced to an ellipse. The laser beam is represented as a collection of parallel rays, with a Gaussian distribution of intensities. Thus the simulation ignores the variation of the beam diameter on the scale of the particle length. Optical forces F and torques Γ are obtained by summing up all the elementary momentum transfers due to the many reflections and refractions of each ray. In the general case F and Γ depend on x, z, θ; but results of [44] were presented in the case of a particle in contact to the top interface, *i.e.* for $z \approx 0$, for simplicity (we later checked that the latter constraint was not essential, similarly to experimental observations). The simulation provides 2-dimensional maps, namely $F(x,\theta)$ and $\Gamma(x,\theta)$. The particle dynamics is obtained from the balance of F and Γ by corresponding hydrodynamic force and torque [44] (see also [52] for more details):

$$\mathbf{F}\cdot\hat{\mathbf{x}} = \gamma_x\,\dot{x}\,, \tag{1}$$

$$\boldsymbol{\Gamma}\cdot\hat{\mathbf{y}} + \tilde{R}\,\theta\,\mathbf{F}\cdot\hat{\mathbf{z}} = -\gamma_\theta\,\dot{\theta}\,, \tag{2}$$

where the dot means time derivative. $\tilde{R}$ is a length given by $\tilde{R} = Rk^{-4/3}\left(k^2-1\right)$, γ_x and γ_θ are Stokes drag coefficients for the motion of the ellipsoid, in translation along $\hat{\mathbf{x}}$ and in rotation around $\hat{\mathbf{y}}$, respectively. Both are functions of R and k, and can be found in [53,54]. The second term in eq. (2) is the torque exerted by the RP force around the point of contact of the particle to the top surface. Note that the above equations only hold in the limit of small particle tilt angle ($\theta \ll \pi/2$).

It is instructive to re-write eqs. (1), (2) using dimensionless quantities. Denoting c the velocity of light in vacuum, we define: $\bar{x} = x/R$, $\bar{z} = z/R$, $\bar{F}_i = cF_i/P$, $\bar{\Gamma} = c\Gamma/PR$, $\bar{\gamma}_x = \gamma_x/\eta R$, $\bar{\gamma}_z = \gamma_z/\eta R$, $\bar{\gamma}_\theta = \gamma_\theta/\eta R^3$, $\bar{t} = t/\tau$ with $\tau = c\eta R^2/P$. Note that the force and torque are proportional to the laser power but the corresponding dimensionless $\bar{F}_i$ and $\bar{\Gamma}$ are independent of P. The dynamical equations now read

$$\bar{F}_x = \bar{\gamma}_x \frac{\mathrm{d}\bar{x}}{\mathrm{d}\bar{t}}\,, \tag{3}$$

$$\bar{\Gamma} + \tilde{R}\theta\bar{F}_z = -\bar{\gamma}_\theta \frac{\mathrm{d}\theta}{\mathrm{d}\bar{t}}\,. \tag{4}$$

From the structure of eqs. (3), (4), the solution can be expressed as: $\bar{x} = X(\bar{t})$, $\theta = \Theta(\bar{t})$. We see that the *amplitude of the oscillations does not depend on the laser power*, which is in line with what we experimentally observed. The power parameter only intervenes through the characteristic time τ. Increasing P only amounts to decreasing the period of oscillations.

Considering $\omega_0 = 1.3\,\mu$m, the simulation successfully reproduces the kind of bifurcation observed in experiments: short ellipsoids ($k < k_C$) get statically aligned on the beam axis, while longer ones oscillate in a periodic manner. Note that the 2-dimensional representation makes sense both for prolate ($k > 1$) and oblate particles ($k < 1$) through the $k \to 1/k$ transformation. Thus the simulation predicts both types of bifurcation, for prolate particles ($k > k_C$) and oblate ones ($k < k_C$). The value of k_C (≈ 4.0 for an S-type polarization, *i.e.* parallel to the plane of incidence) departs from the experimental result (≈ 3.0), but the simulation may be felt as successful as it only pretends to offer qualitative results.

Examples of $F(x,\theta)$ and $\Gamma(x,\theta)$ maps are displayed in fig. 20, for k slightly above the bifurcation threshold.

Our goal, in what follows, is to get some physical insight into the mechanism that makes ellipsoidal particles dance around the beam axis. In practice, we want to spot the main features of the force and torque maps that determine sustained oscillations. For illustration, we examine in fig. 20 a situation close to the threshold for oscillation (S polarization). Blurring out irrelevant details (see S4), we identify a few main features of the maps. These features can be gathered into the picture shown in fig. 21. Essentially the torque function $\Gamma(x,\theta)$ reduces to a couple of positive and negative poles, while the force $F(x,\theta)$ has a

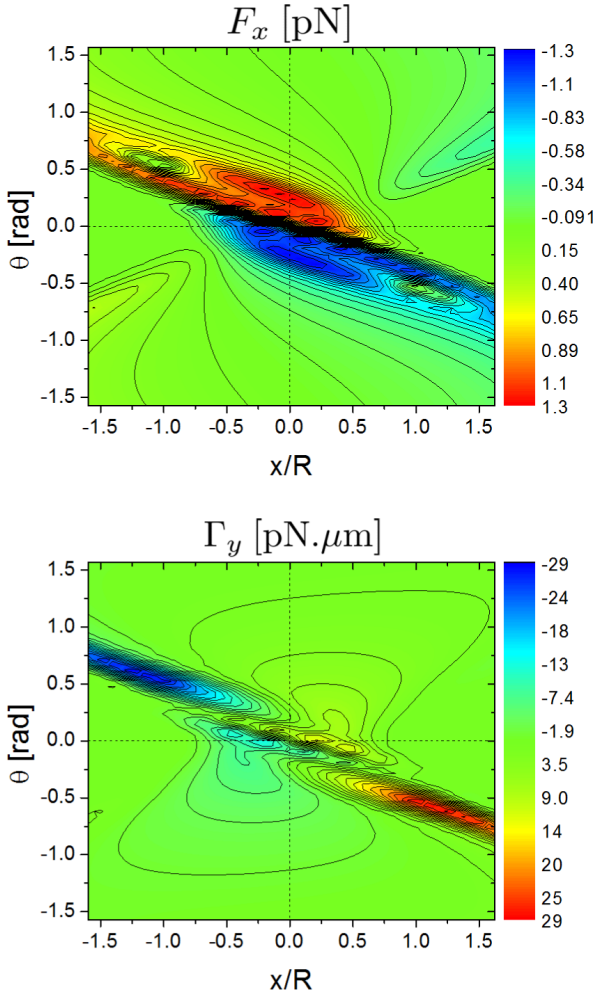

Fig. 20. Computed $F(x,\theta)$ and $\Gamma(x,\theta)$ maps for a collimated beam and aspect ratio $k = 4.1 > k_C$, with $k_C = 4.085$ (S polarization) and beam radius $\omega_0 = 1.3\,\mu$m.

4-pole structure. This overall 6-pole structure forms the basis of the model presented below. Note that the optical force tends to bring the particle back on axis ($x = 0$) only for small tilt angles ($\theta \approx 0$). Conversely, the force becomes repulsive when the tilt increases. In this case the particle is expelled out of the axis, but the torque has a restoring effect in bringing the particle back to vertical. This change in $F(x,\theta)$ together with the action of the torque is the source of the oscillatory response of the particle.

Equations corresponding to the sketch of fig. 21 may be written as

$$G(x)G(\theta-1) - G(x)G(\theta+1) - G(x-1)G(\theta) + G(x+1)G(\theta) = \dot{x}\,, \quad (5)$$

$$A\,[G(\theta+u)G(x-t) - G(\theta-u)G(x+t)] = -\dot{\theta}\,, \quad (6)$$

where $G(x)$ may be defined as a simple Gauss function (only the bell shape of the function is important). $(0,\pm1)$ and $(\pm1,0)$ are the coordinates of the force poles. $(t,-u)$ and $(-t,u)$ are the coordinates of the torque poles, with $t \geq 1$ and $0 < u < 1$.

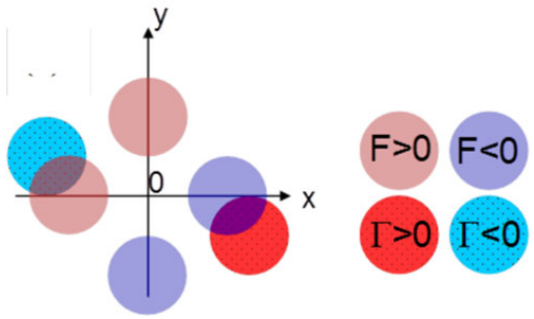

Fig. 21. 4-pole force/2-pole torque model of $F(x,\theta)$ and $\Gamma(x,\theta)$ functions. Graphical codes are defined in the panel on the right.

A is the control parameter of the dynamical system. Physically, A represents the amplitude of the torque, which, as we saw, increases with the aspect ratio k. Linearization of eqs. (5), (6) near $(0,0)$ yields the Jacobian matrix J

$$J = 4\begin{bmatrix} -e^{-1} & e^{-1} \\ -At\,e^{-(t^2+u^2)} & Au\,e^{-(t^2+u^2)} \end{bmatrix}. \quad (7)$$

J may be viewed as the "rigidity matrix" of the system [43]. The off-diagonal elements of J represent the coupling between optical force and torque. Note that the matrix is not symmetrical ($J_{\theta x} \neq J_{x\theta}$), as a consequence of the non-conservative character of the optical forces [43].

For small values of the control parameter ($A < A_C$, see below), corresponding to weakly elongated ellipsoids, $(0,0)$ is a stable fixed point of eqs. (5), (6). The particle is stably trapped on the beam axis ($x = 0$), in vertical configuration ($\theta = 0$)[1].

We find that linear stability is lost when A reaches the threshold value $A_C = u^{-1}e^{t^2+u^2-1}$. There, the system bifurcates from spiral stability to spiral instability. Non-linearities in $F(x,\theta)$ and $\Gamma(x,\theta)$ functions then make the trajectory saturate onto a limit cycle whose amplitude increases with A. Below (fig. 22) we show results from numerical resolution of the above dynamical system, obtained by a fourth-order Runge-Kutta integration. We show examples with ($t = 1$, $u = 0.5$). With these values, the torque poles have same abscissas as those of the horizontal force dipole. We checked that this case had nothing special by testing with other values ($t > 1$, $u \neq 0.5$). Computation time considerably increases with t, but we find the same trends (bifurcation and limit cycles) in all cases.

Summarizing, the 4-pole force/2-pole torque model, represented by eqs. (5), (6), produces the kind of bifurcation that has emerged from the simulation. The key parameter that drives the bifurcation is the amplitude of the torque, represented by the A parameter in eq. (6). Note that the instability, and then the onset of oscillations, only

[1] To be complete, eqs. (5), (6) should include a random (Langevin) force, to account for thermal noise. The latter will make the ellipsoid undergo Brownian excursions in position and tilt angle with specific statistical properties [43].

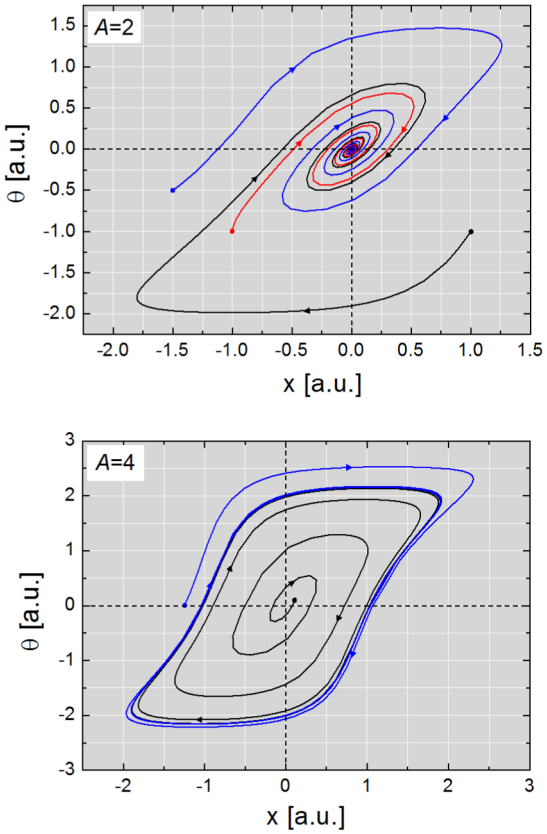

Fig. 22. Trajectories obtained by integration of eqs. (5), (6), below (a) and above the transition (b). Here $t = 1$, $u = 0.5$.

exists for finite values of u. Coming back to maps (fig. 20), a necessary condition for the system to oscillate is that the torque poles have to be shifted from the force poles. Otherwise stated, the force and the torque change their signs at different positions in (x, θ). We refer the readers to a detailed discussion on this issue in our Part II article [52].

In the above pole model, the bifurcation is continuous (of super-critical Hopf type), meaning that the extent of the limit cycle grows continuously starting from zero at $A = A_C$. The simulation instead indicates a discontinuous transition, with possibly coexisting static and oscillating states above A_C [44] (see also Part II [52]). However the difference is not essential as it may be explained if one takes into account fine features of the force-torque maps near $(0, 0)$, which are not present in fig. 21; see S4 for a detailed justification.

5 Discussion and concluding remarks

We have described the mechanical effects of a laser beam on large size (up to several $10\,\mu$m in length) ellipsoidal polystyrene particles in water. In our experiments, the beam was moderately focused, meaning that beam diffraction was weak on the scale of the particles. We observed that particles that were not far from spherical, namely prolate ellipsoids with $k < 3$ or oblate ones with $k > 0.33$, would get radially trapped on the beam axis, with their long side lying parallel to the beam. Conversely particles sufficiently far from spherical, *i.e.* elongate ($k > 3$) or flat ($k < 0.33$), would not be trapped or repelled from the laser beam, but would rather undergo sustained oscillations. Importantly the oscillations were observed in general, be the particle in bulk water, in a simple levitation scheme, or in contact with an interface. Tests with fluid (water-oil, water-air) or solid (water-glass) interfaces did not reveal qualitative differences, as oscillations were observed in all cases.

Referring to basic principles of mechanical effects of light on matter, particularly the non-conservative character of optical forces [42,43], the existence of the oscillations does not come as a surprise, since nothing imposes the particle to come to a static equilibrium inside (as in optical trapping) or outside (simple repulsion) of the beam. The benefit of the experiments with the PS ellipsoids is their simplicity to illustrate the fact that dynamical equilibria should be encountered in certain experimental conditions.

Based on our observations and a recent simulation in 2 dimensions, we proposed a qualitative model to understand why the particles oscillate. The simulation indicates that the oscillations originate from the structure of the optical force and torque maps, and that the torque amplitude A is the bifurcation control parameter. In general, tilting the particle results in the particle being expelled out of the beam, and pushing the particle off-axis make it rotate in a way that worsens the initial tilt in θ. Thus the force-torque coupling, represented by the off-diagonal terms in J, has a destabilizing effect, while the diagonal terms are stabilizing. The amplitude of the torque rules the competition between both tendencies. For moderate k (< 4 in S polarization), the torque is weak and the particle is axially trapped in $(x = 0, \theta = 0)$ configuration; while for high k the particle is expelled out of the beam. In the latter case the instability saturates due to the nonlinear forms of $F(x, \theta)$ and $\Gamma(x, \theta)$ functions, resulting in cyclic motion of the particle.

The above results from the simulation, as we said, have been limited to a parallel beam and to one particular value of the beam diameter. In spite of the intrinsic limitation of the model (ray-optics and dimension 2), it is worth exploring the effects of changing the beam parameters, namely ω_0 and the beam divergence. This forthcoming work, the matter of a second part article [52], should help us understand some of the observations reported in subsect. 3.3, and may be useful in predicting anisotropic particles behaviours in high aperture beams, such as used in optical tweezers geometries.

In experimental records and in the model we limited the description of the system to a couple of coordinates, namely x and θ. Strictly speaking, the physical system is $2d$ only if the particle is axisymmetrical, and if the particle and laser beam symmetry axes are coplanar (providing cylindrical symmetry to the whole system). In many cases, the real system did not meet these conditions, and then was $3d$, with a corresponding 5-dimensional configuration space. Indeed a large part of the data displayed in fig. 15

corresponds to $3d$ systems. This may be the reason why domains corresponding to different states in fig. 15 slightly overlap, instead of having neat transition lines. In spite of this complication, the diagram makes a very clear distinction between static and oscillating states. In this context the $2d$ model is sufficient as a minimal basis to understand the origin of oscillations.

Recall that we have ignored the effects of Brownian motion in the model and the simulations. Thermal noise is visible in experiments as very small random excursions of particles. As thermal excursions are much smaller than optically driven oscillations, we believe that they do not have a strong influence on the observed bifurcations. Nevertheless thermal fluctuations may play a role in destabilizing the on-axis configuration above k_C. This may explain why coexistence of static and oscillating states is not observed in experiments up to now.

As a final remark, we note that the simulation, being limited to dimension 2, misses some of the experimental observations that clearly indicate 3-dimensional motion in certain cases with non-axisymmetrical particles. A further limitation lies in the fact that we only considered 2 variables (x and θ), making the dynamical system 2-dimensional. Consequently, limit cycles that come out of the computations can only be periodic [55,56]. The model is then unable to account for irregular signals such in figs. 12, 14, 17, 18. This limitation calls for a generalisation of the simulation in 3 dimensions.

This work has been financially supported by the European ITN program "COMPLOIDS" (2009-2013) and is currently continued under the "AMOCOPS" project (ANR-13-BS09-008) of the Agence Nationale de la Recherche. The authors thank J. Elezgaray, F. Ren, M. Tondusson and J.-P. Galaup for fruitful discussions, and are grateful to CRPP instrumentation and mechanics teams for their continuous help.

References

1. A. Ashkin, Phys. Rev. Lett. **24**, 156 (1970).
2. A. Ashkin, *Optical trapping and manipulation of neutral particles using lasers* (World Scientific, London, 2006).
3. G. Roosen, C. Imbert, Phys. Lett. A **59**, 6 (1976).
4. A. Ashkin *et al.*, Opt. Lett. **11**, 288 (1986).
5. K.C. Neuman, S.M. Block, Rev. Sci. Instrum. **75**, 2787 (2004).
6. A. Jonáš, P. Zemánek, Electrophoresis **29**, 4813 (2008).
7. G. Roosen, PhD thesis, University Paris XI (1978).
8. T.N. Buican *et al.*, Proc. SPIE **1063**, 190 (1989).
9. D.J. Vossen *et al.*, Rev. Sci. Instrum. **75**, 2960 (2004).
10. P.J. Rodrigo, V.R. Daria, J. Glückstad, J. Opt. Lett. **29**, 2270 (2004).
11. P.J. Rodrigo *et al.*, Opt. Express **13**, 6899 (2005).
12. P. Kraikivski, B. Pouligny, R. Dimova, Rev. Sci. Instrum. **77**, 113703 (2006).
13. K.T. Gahagan, G.A. Swartzlander Jr., Opt. Lett. **21**, 827 (1996).
14. K.T. Gahagan, G.A. Swartzlander Jr., J. Opt. Soc. Am. B **15**, 524 (1998).
15. J. Arlt, M.J. Padgett, Opt. Lett. **25**, 191 (2000).
16. V.G. Shvedov, Opt. Express **19**, 17350 (2011).
17. C. Alpmann *et al.*, Appl. Phys. Lett. **100**, 111101 (2012).
18. P.H. Jones, O.M. Maragò, E.P.J. Stride, J. Opt. A: Pure Appl. Opt. **9**, S278 (2007).
19. S.H. Simpson, S. Hanna, J. Opt. Soc. Am. A **27**, 1255 (2010).
20. J.N. Wilking, T.G. Mason, EPL **81**, 58005 (2008).
21. A. Neves *et al.*, Opt. Express **18**, 822 (2010).
22. P.J. Pauzauskie *et al.*, Nat. Mater. **5**, 97 (2006).
23. A. Van der Horst *et al.*, Opt. Express **15**, 11629 (2007).
24. J. Plewa, Opt. Express **12**, 1978 (2004).
25. O.M. Maragò *et al.*, Nat. Nanotechnol. **8**, 807 (2013).
26. M.E.J. Friese *et al.*, Appl. Phys. Lett. **78**, 547 (2001).
27. P.B. Bareil, Y. Sheng, Opt. Express **18**, 26388 (2010).
28. S.H. Simpson, S. Hanna, J. Opt. Soc. Am. A **28**, 850 (2011).
29. R.C. Gauthier, J. Opt. Soc. Am. B **14**, 3323 (1997).
30. R.C. Gauthier, M. Ashman, C.P. Grover, Appl. Opt. **38**, 4861 (1999).
31. S.H. Simpson, S. Hanna, J. Opt. Soc. Am. A **24**, 430 (2007).
32. S.H. Simpson, S. Hanna, Phys. Rev. A **84**, 053808 (2011).
33. H. Sosa-Martínez, J.C. Gutiérrez-Vega, J. Opt. Soc. Am. B **26**, 2109 (2009).
34. F. Borghese *et al.*, Phys. Rev. Lett. **100**, 163903 (2008).
35. Y. Cao *et al.*, Opt. Express **20**, 12987 (2012).
36. M. Rodriguez-Otazo *et al.*, Appl. Opt. **48**, 2720 (2009).
37. T. Imasaka *et al.*, Anal. Chem. **67**, 1763 (1995).
38. C.B. Chang *et al.*, Opt. Express **20**, 24068 (2012).
39. Z. Cheng, P.M. Chaikin, T.G. Mason, Phys. Rev. Lett. **89**, 108303 (2002).
40. Z. Cheng, T.G. Mason, P.M. Chaikin, Phys. Rev. E **68**, 051404 (2003).
41. S.C. Grover, R.C. Gauthier, A.G. Skirtach, Opt. Express **7**, 533 (2000).
42. A. Ashkin, J. Biophys. **61**, 569 (1992).
43. S.H. Simpson, S. Hanna, Phys. Rev. E **82**, 031141 (2010).
44. B.M. Mihiretie, P. Snabre, J.-C. Loudet, B. Pouligny, EPL **100**, 48005 (2012).
45. C.C. Ho *et al.*, Colloid Polym. Sci. **271**, 469 (1993).
46. J.A. Champion, Y.K. Katare, S. Mitragotri, Proc. Natl. Acad. Sci. U.S.A. **104**, 11901 (2007).
47. S.M. Block, *Optical Tweezers: A New Tool for Biophysics*, in *Noninvasive Techniques in Cell Biology*, edited by B.H. Satir (Wiley-Liss, New York, 1990) pp. 375-402.
48. R. Hegger, H. Kantz, T. Schreiber, Chaos **9**, 413 (1999).
49. J.-C. Loudet *et al.*, Phys. Rev. Lett. **94**, 018301 (2005).
50. D.M. Kaz *et al.*, Nat. Mater. **11**, 138 (2012).
51. T.F. Quatieri, *Discrete-Time Speech Signal Processing: Principle and Practice* (Prentice Hall PTR, 2002).
52. J.-C. Loudet, B.M. Mihiretie, B. Pouligny, Eur. Phys. J. E **37**, 125 (2014).
53. J. Happel, H. Brenner, *Low Reynolds Number Hydrodynamics* (Kluwer, Dordrecht, 1991).
54. Y. Han *et al.*, Phys. Rev. E **80**, 011403 (2009).
55. R. Rosen, *Dynamical System Theory in Biology*, Vol. **1** (Wiley-Interscience, 1970).
56. J.M.T. Thompson, H.B. Stewart, *Nonlinear Dynamics and Chaos* (John Wiley & Sons, 1986).